Comparison of Cell Homogenization Methods Considering Interaction Effect Between Fuel Cells and Control Rod Cells

Toshikazu Takeda and Nariaki Uto

Osaka University*, Faculty of Engineering
Department of Nuclear Engineering

*Yamada-oka 2-1, Suita, Osaka

ABSTRACT

Several methods to determine cell-averaged group cross sections and anisotropic diffusion coefficients which consider the interaction effect between core fuel cells and control rods or control rod followers have been compared to discuss the physical meaning included in cell homogenization. As the cell homogenization methods considered are the commonly used flux-weighting method,the reaction rate preservation method and the reactivity preservation method. These homogenization methods have been applied to control rod worth calculations in 1-D slab cores to investigate their applicability.

1. INTRODUCTION

Cell homogenization has been studied for many years to obtain cell-averaged cross sections and anisotropic diffusion coefficients(DC). The most popular procedure which is often used in fast reactor core analysis is to perform infinite cell calculations and to obtain the flux-weighted cell-averaged cross sections and Benoist anisotropic DC.

This procedure produces errors when applied to the super-cell model composed of core cells and singular cells such as control rods, sodium followers, blanket cells because of the neglect of the interference between core cells and singular cells.

To treat the interference we proposed a homogenization method which preserves reaction rates in each energy group[1]. Furthermore to consider the neutron streaming we extended the Benoist's formula to the supercell model.[2] The cell-averaged cross section was applied to control-rod worth prediction of fast reactor, and the verification of this procedure was performed.[1] The extended Benoist DC was applied to sodium void worth calculation; The calculated sodium void worth was in good agreement with that evaluated by transport theory calculation.[3] This result indicates that not only the neutron streaming effect in a cell but also the local transport effect in the supercell model are included in the extended Benoist DC. Therefore the calculated result need not be transport corrected otherwise the transport correction is doubly considered.

Thus it is necessary to investigate the extended Benoist formula from the theoretical point and manifest the physical meanings included in the formula. Furthermore, it is desirable to derive a formula for an anisotropic DC which is useful for transport theory calculations. In this case the neutron streaming effect in each cell consisting a supercell has to be considered, but the transport effect over the supercell should not be included.

For the purpose we compare the cell-averaged cross sections and DCs obtained from the reaction rate preservation method and the reactivity preservation method. The reactivity preservation method was first derived by Rowlands-Eaton[4] and this method has been successfully utilized in FBR control rod worth calculations

by Salvatores et al,[5] who included the transport and mesh size effects in the homogenized cross sections. In the two methods, the reaction rate and/or the reactivity of each cell is preserved after the cell homogenization. The reaction rate or reactivity for the as-built heterogeneous cell before the cell homogenization has to be calculated by transport theory, but that after the cell homogenization can be calculated by both transport and diffusion theories. When diffusion theory is used, the transport effect over the supercell used is included in the group constants. On the other hand, when transport theory is used, the intra-cell transport effect is included in the homogenization. The derived transport cross section includes the neutron streaming effect within a cell. Thus, from the comparison we can find what physical meanings are included in the extended Benoist diffusion coefficient. Furthermore we can find out an expression for an anisotropic DC which includes only the neutron streaming effect.

Chapter II describes the cell homogenization methods from these theoretical points.

To illustrate the difference of various cell homogenization methods, we apply them to supercell models consisting of core fuel and control rod, core fuel and control rod position. Chapter III compares cell-averaged cross sections obtained from the flux-weighting method, the reaction rate preservation method and the reactivity preservation method. The control rod worths calculated by these methods in 1-D slab systems are also compared to investigate their applicability.

2. COMPARISON OF CELL HOMOGENIZATION

Let us derive the cell-averaged cross sections and diffusion coefficients obtained from the reaction rate and/or reactivity preservation methods.

In the reaction rate preservation method, the cell averaged cross sections are obtained by iterations such that the homogenized cross section time the flux calculated by the cross section is equal to the original reaction rate obtained by a heterogeneous supercell calculation, within a certain criterion. Thus, the cell-averaged cross section is defined by

$$\Sigma^{*g} = \frac{\int_{cell} d\vec{r}\ \Sigma^g(\vec{r})\varphi^g(\vec{r})}{\int_{cell} d\vec{r}\ \varphi^g_{homo}(\vec{r})} \qquad (1)$$

where $\varphi^g_{homo}(\vec{r})$ is the flux calculated by Σ^{*g}. When we use diffusion theory and transport theory in calculating $\varphi^g_{homo}(\vec{r})$, we obtain the group constants which preserve original reaction rates by diffusion and transport calculations, respectively. This reaction rate preservation method is rather simple, and effective in homogenizing cells with strong heterogeneity. Thus it has been utilized in the control rod worth calculation.[1] However the method can not take into account the neutron streaming in a cell; the cell-averaged transport cross section in an infinite lattice becomes the flux weighted cross section; the $1/3\ \Sigma^{*g}_{tr}$ does not

reduce to the Benoist DC.

In the reactivity preservation method, different expressions are obtained dependent on the use transport and diffusion theories.

With the transport theory for the cell homogenization, the cell-averaged absorption, scattering, fission and transport cross sections are defined by

$$\Sigma_a^{*g} = \frac{\int_{cell} d\vec{r}\ \Sigma_a^g(\vec{r})\Phi_0^g(\vec{r})\Psi_0^{*g}(\vec{r})}{\int_{cell} d\vec{r}\ \Phi_0^g(\vec{r})\Psi_0^{*g}(\vec{r})} \tag{2}$$

$$\Sigma_s^{*g\to g'} = \frac{\int_{cell} d\vec{r}\ \Sigma_s^{g\to g'}(\vec{r})\Phi_0^g(\vec{r})[\Psi_0^{*g'}(\vec{r})-\Psi_0^{*g}(\vec{r})]}{\int_{cell} d\vec{r}\ \Phi_0^g(\vec{r})[\Psi_0^{*g'}(\vec{r})-\Psi_0^{*g}(\vec{r})]} \tag{3}$$

$$\Sigma_f^{*g} = \frac{\int_{cell} d\vec{r}\ \Sigma_f^g(\vec{r})\Phi_0^g(\vec{r})\sum_{g'}\chi^{g'}\Psi_0^{*g'}(\vec{r})}{\int_{cell} d\vec{r}\ \Phi_0^g(\vec{r})\sum_{g'}\chi^{g'}\Psi_0^{*g'}(\vec{r})} \tag{4}$$

$$\Sigma_{tr}^{*g} = \frac{\int_{cell} d\vec{r}\int_{4\pi} d\vec{\Omega}\ \Sigma_{tr}^g(\vec{r})[\Phi^g(\vec{r},\vec{\Omega})-\frac{1}{4\pi}\Phi_0^g(\vec{r})]\Psi^{*g}(\vec{r},\vec{\Omega})}{\int_{cell} d\vec{r}\int_{4\pi} d\vec{\Omega}\ [\Phi^g(\vec{r},\vec{\Omega})-\frac{1}{4\pi}\Phi_0^g(\vec{r})]\Psi^{*g}(\vec{r},\vec{\Omega})} \tag{5}$$

where $\Phi_0^g(\vec{r})$ and $\Psi_0^{*g}(\vec{r})$ are the flux distribution in a heterogeneous cell and the adjoint flux distribution in the homogenized cell. The cross sections (2)~(5) require the calculation of the adjoint flux, therefore we have to repeat the adjoint flux calculation and the homogenization of cross sections until they converge. These are calculated based on transport theory. The derivation is shown in Appendix.

The adjoint angular distribution after the cell homogenization is well represented by the P_1 approximation. Using the P_1 approximation to Eq.(5) and defining the direction dependent transport cross section so as to preserve the leakage in each direction, we obtain

$$\Sigma_{tr,k}^{*g} = \frac{\int_{cell} d\vec{r}\ \Sigma_{tr}^g(\vec{r})\Phi_{1k}^g(\vec{r})\Psi_{1k}^{*g}(\vec{r})}{\int_{cell} d\vec{r}\Phi_{1k}^g(\vec{r})\Psi_{1k}^{*g}(\vec{r})} \tag{6}$$

where $\Phi_{1k}^g(\vec{r})$ and $\Psi_{1k}^{*g}(\vec{r})$ are the P_1 components of the normal and adjoint angular distributions, respectively.
The diffusion coefficient D_k^g is defined by

$$D_k^g = 1/3\Sigma_{tr}^{*g} \tag{7}$$

Thus defined anisotropic diffusion coefficients are suitable to the analysis of fast reactor cores, because the neutron

performance parameters are usually evaluated by performing diffusion calculations with anisotropic diffusion coefficients and by adding the transport correction obtained using the transport cross section Σ_{tr} related to the diffusion coefficient D by $\Sigma_{tr}=1/3D$.

In the heterogeneous lattice consisting of one-dimensional slab cells, we can derive the perpendicular and parallel DCs from Eq.(6) as shown in Appendix.

$$D_{\perp}^{*g} = \frac{\sum_{i\in cell} \varphi_{1x,i}^{g} \psi_{1x,i}^{*g} V_i}{3 \sum_{i\in cell} \Sigma_{tr,i}^{g} \varphi_{1x,i}^{g} \psi_{1x,i}^{*g} V_i} \tag{8}$$

$$D_{//}^{*g} = \frac{\sum_{i\in cell}^{super} \sum_{j\in cell} \varphi_i^g V_i P_{ij,z}^g / \Sigma_{tr,j}^g}{3 \sum_{i\in cell}^{super} \sum_{j\in cell} \varphi_i^g V_i P_{ij,z}^g} \tag{9}$$

With the diffusion theory, the cell-averaged absorption, scattering and fission cross sections have the same expressions as Eqs.(2)~(4) except that the homogenized adjoint flux is calculated by diffusion.[1] However the anisotropic diffusion coefficient is defined by

$$D_k^{*g} = -\frac{\int_{cell} d\vec{r}\ \psi_0^{*g}(\vec{r}) \frac{\partial}{\partial k} \varphi_{1k}^{g}(\vec{r})}{\int_{cell} d\vec{r}\ \varphi_0^{g}(\vec{r}) \frac{\partial^2}{\partial k^2} \psi_0^{*g}(\vec{r})} \tag{10}$$

In the supercell consisting of one-dimensional slab cells in x-axis, the perpendicular($D_{\perp}$) and parallel($D_{//}$) DCs are derived from Eq.(10).[1]

$$D_{\perp}^{*g} = -\frac{\int_{cell} dx\ \varphi_{1x}^{g}(x) \frac{d}{dx} \psi_0^{*g}(x)}{\int_{cell} dx \frac{d}{dx}\varphi_0^{g}(x) \frac{d}{dx} \psi_0^{*g}(x)} \tag{11}$$

$$D_{//}^{*g} = \frac{\sum_{i\in cell}^{super} \sum_{j\in cell} \varphi_i^g V_i P_{ij,z}^g / \Sigma_{tr,j}^g}{3 \sum_{j\in cell} \varphi_j^g V_j} \tag{12}$$

The perpendicular DCs, Eqs.(8) and (11) derived based on transport and diffusion theories include the P_1 component of the angular flux, and they are different from Benoist DC. The parallel DCs, Eqs.(9) and (12) are similar to each other. Eq.(12) corresponds to the extended Benoist DC.

To clearify the difference we apply them to a simple supercell model consisting of two homogeneous cells denoted by suffixes 1 and 2. Eq.(9) leads to the homogeneous limit :

$$D_{k,tr}=1/3\Sigma_{tr,1} \quad \text{for cell 1}$$
$$=1/3\Sigma_{tr,2} \quad \text{for cell 2} \tag{13}$$

However, the extended Benoist DC, Eq.(12) leads to the following expression.

$$D^g_{k,ex} = \frac{1}{3\Sigma^g_{tr,i}} \left[P^g_{11,k} + P^g_{21,k} \frac{\varphi^g_2 V_2}{\varphi^g_1 V_1} \right] \tag{14}$$

Thus, the extended Benoist's formula contains the interference term ; which is caused by the local transport effect. Therefore the use of this diffusion coefficient in diffusion calculations and the adoption of the transport correction takes into account the local transport effect twice.

3. NUMERICAL RESULTS OF CELL INTERACTION EFFECTS

Let us first compare numerical results of cell-averaged cross sections and DCs for the cells used in the fast critical assembly ZPPR. In ZPPR, there are two types of fuel drawers, blanket drawers, and singular drawers such as sodium followers (CRP), control rods (CR). To treat the interaction between these cells we consider four supercell models,(a)~(d), shown in Fig. 1; models (a) and (b) contain CRP drawer and models (c) and (d) contain CR drawer. Furthermore, we consider the case when the B_4C plates are lumped at the CR cell center as shown in Fig. 1. The supercell models similar to the models (c) and (d) with this CR are indicated by (c') and (d').

All the supercell calculations were performed in 7 energy groups using macroscopic cross sections produced from JENDL-2. The energy structure is shown in Table I. The following four homogenization methods are used to calculate the cell averaged cross sections.

(1) infinite cell calculation: cell-averaged cross sections being calculated with the flux as weight and DC being calculated using Benoist's formula; the flux in the singular cells is calculated using the supercell models
(2) supercell calculation: cell-averaged cross sections being calculated with the flux as weight; DC being calculated using the extended Benoist's formula
(3) supercell calculation using the reaction rate preservation method: cell-averaged cross sections (including transport cross section) being calculated from Eq.(1); DC being calculated from $1/3\Sigma_{tr}$
(4) supercell calculation using the reactivity preservation method: cell-averaged cross sections being calculated from Eqs.(2)~(4); DC being calculated from $1/3\Sigma_{tr}$

where Σ_{tr} is calculated from Eq.(5).

All the cell and supercell calculations were performed using S_{16} P_0 approximation with 42 spatial meshes in a fuel drawer and 50 spatial meshes in a CR or CRP drawer. After these homogenization calculations the supercell calculations are performed with thus obtained homogenized cross sections, and the results are compared with the reference heterogeneous calculation.

Table II lists the k_{eff} values for the supercell transport calculations with the homogenized cross sections obtained from the four cell homogenization methods as well as the reference heterogeneous calculation which treats the plate-by-plate heterogeneity. The use of the homogenized cross section from the infinite cell calculation produces large errors. These errors are reduced when we consider the cell interaction by using homogenization method (2). The reaction rate preservation method, method (3), gives very accurate results for the all cases considered. The reactivity preservation method gives more accurate results compared to the method (2), but the error is rather large for all models. This is because the homogenization procedure requires the anisotropic angular flux and numerical errors are large. The iteration number to get the homogenized cross sections is about 6 and 7 for the reaction and reactivity preservation methods.

Next let us compare the DCs and cell-averaged cross sections obtained from the four homogenization methods. Tables III and IV list the DCs for the models (b) and (d) for the four homogenization methods. For the fuel drawer not adjacent to CRP in the model (b), the reactivity preservation method led to a numerical problem; the term in the bracket [ ] in Eq.(5) is very small. Then we replaced the term by $\Phi_0^g(\vec{r})$ only for the fuel. The values in Tables III and IV are the percent difference from $1/3\,\Sigma_{tr}$ where Σ_{tr} is the flux weighted transport cross section obtained from infinite cell calculations. The deviation is small for the Benoist formula. The extended Benoist DC is remarkably different from the Benoist DC calculated in infinite cell calculations. It is larger than the infinite-cell Benoist DC over 10% for the fuel adjacent to CRP, though the increase is rather small for the fuel not adjacent to CRP. Oppositely the extended Benoist DC is smaller than $1/3\,\Sigma_{tr}$ over by 10% in the CRP above 100 kev. The reverse is observed for the models (c) and (d), which include CR: The extended Benoist DC is smaller than the infinite-cell Benoist DC above 1Mev (see Table IV) for the fuel adjacent to CR. Thus, the extended Benoist DC differs remarkably from $1/3\,\Sigma_{tr}$ depending on the type of singular cells. This difference includes the spatial transport effect around the singular drawer.

The reaction rate preservation method does not yield the anisotropic DC. The evaluated DC is smaller than $1/3\Sigma_{tr}$ for the fuel drawers and larger for the CRP and CR drawers above 1Mev. This difference corresponds to that for the cell-averaged absorption and fission cross sections as will be shown in Tables VI and VII.

The reactivity preservation method yields larger $D_\perp$ values compared to $1/3\Sigma_{tr}$ for the fuel drawers adjacent to CRP or CR at

the high energy groups. The same trend is seen for the CRP and CR drawers. When we use the approximate Eq.(8) in the estimation of $D_\perp$ instead of Eq.(5), some error is introduced. Table V shows the difference for the fuel drawer of the model (a). The use of Eq.(8) underestimates the difference of $D_\perp$ from $1/3\,\Sigma_{tr}$.

In the following we compare the cell-averaged absorption and production cross sections obtained from the four homogenization methods. Table VI and VII list the percent difference of the cell-averaged cross sections obtained by the supercell flux weighting method, the reaction rate preservation method, and the reactivity preservation method from the infinite cell calculations for the supercell models (b) and (d), respectively.

The values for CRP and CR are the differences from the supercell flux weighting method because the infinite cell calculation is not available for such drawers.

The supercell flux weighting method and the reactivity preservation method yield the similar results for fuel drawers and CRP. This implies that the adjoint flux distribution appearing as the weight in Eqs.(2) (4) has a small effect: If $\psi_0^{*g}(r)$ is constant, Eqs.(2) and (4) reduce to the flux weighted cell averaged cross sections. However, for the CR drawer the reactivity preservation method yields different results from the supercell flux weighting method because of the strong adjoint flux variation in the CR drawer.

The reaction rate preservation method leads to larger cell-averaged cross sections for fuel drawers compared to the flux-weighting method above 1MeV. Particularly, the production cross sections of the 1'st group for the fuel drawers adjacent to CRP and CR, are larger than the those from the infinite cell calculation by 6.5~7.6%. While the absorption cross sections for CRP and CR are smaller than the flux-weighting procedure, especially in the 1'st group (5~9%). This decrement of the absorption cross section, especially for CR, corrects the overestimation of the control rod worth evaluated by the flux-weighting method.

We have applied the these homogenization methods to control rod worth calculations in a 1-D slab model. The 1-D slab model is shown in Fig. 2. The control rod worths and k_{eff} for CR with separate B_4C plates calculated are listed in Table VIII. The supercell calculations were performed two drawer models: models(a) and (c) in Fig.1. The infinite cell calculation model leads to rather larger control rod worth. The use of supercell model, the reaction rate and reactivity preservation methods, all give reasonable results. The use of the extended Benoist DC leads to an underestimation of control rod worth as expected. The use of 3-drawer model produces the similar results as for the 2-drawer model.

Table IX lists the control rod worth and k_{eff} for CR with lumped B_4C plates. In this case, the supercell flux weighting procedure overestimates the control rod worth. The use of the reaction rate and the reactivity preservation methods lead to reasonable results. The reactivity preservation method leads to a little overestimation for the off center control rod worth. This is due to the fact that, when the off center control rod is

inserted, the fast group flux in the fuel regions around the core center is underestimated. In the reactivity preservation method, the self-scattering cross section cannnot be defined because both the numerator and the denominator in Eq.(3') become exactly zero. This may cause some problems in reactor analysis based on transport theory. Furthermore, we found some problems in convergence of the transport cross section, in particular, for the cell where the angular flux is nearly isotropic and for the control rod drawer.

4. CONCLUSIONS

We have compared the cell homogenization method for the estimation of cell interaction effect, the supercell flux weighting method, the reaction rate preservation method and the reactivity preservation method.

The numerical results of cell-averaged cross sections and DC have been compared. The control rod worths for 1-D slab ares were calculated for these methods and compared with a reference one. The reaction rate preservation method was stable and lead to reasonable results.

REFERENCES

[1] TAKEDA,T.,SATO,H. and ONO,S., An Effective Homogenization Method for Heterogeneous Assemblies, Ann. nucl. Energy,9, 509 (1982).

[2] TAKEDA,T., ARAI,K. and YAMAOKA,M., Unified Diffusion Coefficient for Analysis of Sodium-Void Worth in Fast Critical Assembly with Control-Rod Channels, J. Nucl. Sci. Technol. , 18, 93 (1981).

[3] TAKEDA,T. and YAMAMOTO,T., Sensitivity Coefficients for Leakage and Nonleakage Components of Sodium Void Worth, Nucl. Sci. Eng. ,87, 80 (1984).

[4] ROWLANDS,J.L. and EATON,C., The Spatial Averaging of Cross Sections for use in Transport Calculations, with an Application to Control Rod Fine Structure Homogenization , Proc. IAEA Specialists Meeting on Homogenization Methods, Lugano (1978).

[5] SALVATORES,M. et al, Development of a Common European Scheme for Fast Reactor Core Calculations From Basic Data to Experimental Validation , Proc. 1988 International Reactor Physics Conference, Jackson Hall Wyoming. Sep. 18-22, 1988.

[6] TAKEDA,T. and OOE,T., Determination of Cell Averaged Diffusion Constants Based on Transport/Diffusion Perturbation Theory, J. Nucl. Sci. Technol. ,24, 999 (1987).

APPENDIX

We consider the cell homogenization as perturbation. Then the transport equation before perturbation is

$$\vec{\Omega}\cdot \mathrm{grad}\,\Phi^{g}(\vec{r},\vec{\Omega}) + \Sigma^{g}_{tr}(\vec{r})\,\Phi^{g}(\vec{r},\vec{\Omega}) = \frac{1}{4\pi}\sum_{g'}\Sigma_{s}^{g'\to g}(\vec{r})\,\Phi_{0}^{g'}(\vec{r}) + \frac{\chi^{g}}{4\pi k_{eff}}\sum_{g'}\nu\Sigma_{f}^{g'}(\vec{r})\,\Phi_{0}^{g'}(\vec{r}) \qquad (A.1)$$

where $\Phi^{g}(\vec{r},\vec{\Omega})$: g-group neutron angular flux at point $\vec{r}$ along direction $\vec{\Omega}$,
$\Phi_{0}^{g}(\vec{r})$: P_0 component of the g-group angular flux,
$\Sigma_{x}^{g}(\vec{r})$: g-group cross section of type x (tr:transport, s:scattering, f:fission) at point $\vec{r}$ in a heterogeneous cell,
χ^{g} : g-group fission spectrum,
and the isotropic scattering is assumed.

The adjoint transport equation after perturbation is

$$-\vec{\Omega}\cdot \mathrm{grad}\,\Psi^{*g}(\vec{r},\vec{\Omega}) + \Sigma^{*g}_{tr}(\vec{r})\,\Psi^{*g}(\vec{r},\vec{\Omega}) = \frac{1}{4\pi}\sum_{g'}\Sigma_{s}^{*g\to g'}(\vec{r})\,\Psi_{0}^{*g'}(\vec{r}) + \frac{\nu\Sigma_{f}^{*g'}(\vec{r})}{4\pi k^{*}_{eff}}\sum_{g'}\chi^{g'}\Psi_{0}^{*g'}(\vec{r}) \qquad (A.2)$$

where $\Psi^{*g}(\vec{r},\vec{\Omega})$: g-group adjoint angular flux after the cell homogenization at point $\vec{r}$ along direction $\vec{\Omega}$,
$\Psi_{0}^{*g}(\vec{r})$: P_0 component of the adjoint angular flux,
$\Sigma_{x}^{*g}(\vec{r})$: g-group cross section of type x at point r in a homogenized cell.

Multiplying Eq.(A.2) by $\Phi^{g}(\vec{r},\vec{\Omega})$ and Eq.(A.1) by $\Psi^{*g}(\vec{r},\vec{\Omega})$, substracting the resultant equations and integrating over all solid angles, volume and energy groups lead to the following :

$$\begin{aligned}\frac{\Delta k_{eff}}{k_{eff}\,k^{*}_{eff}} = \frac{1}{N}\sum_{g}\Big[& -\int_{cell} d\vec{r}\int d\vec{\Omega}\,\{\Sigma^{*g}_{tr}-\Sigma^{g}_{tr}(\vec{r})\}\,\Psi^{*g}(\vec{r},\vec{\Omega})\,\Phi^{g}(\vec{r},\vec{\Omega}) \\ & + \frac{1}{4\pi}\int_{cell} d\vec{r}\sum_{g'}\Sigma_{s}^{*g-g'}(\vec{r})\,\{\Psi_{0}^{*g'}(\vec{r})\,\Phi_{0}^{g}(\vec{r}) - \Sigma_{s}^{g'-g}\Psi_{0}^{*g}(\vec{r})\,\Phi_{0}^{g'}(\vec{r})\} \\ & + \frac{1}{4\pi}\int_{cell} d\vec{r}\sum_{g'}\chi^{g'}\Psi_{0}^{*g'}(\vec{r})\,\{\nu\Sigma_{f}^{*g}\,\Phi_{0}^{g}(\vec{r}) - \nu\Sigma_{f}^{g}\Phi_{0}^{g}(\vec{r})\}\Big]\end{aligned} \qquad (A.3)$$

where $N = \int_{cell} d\vec{r}\sum_{g}\nu\Sigma_{f}^{g}(\vec{r})\,\Phi_{0}^{g}(\vec{r})\sum_{g'}\chi^{g'}\Psi_{0}^{*g'}(\vec{r})$.

We add the following to the second term and substract it from the first term,

$$\begin{aligned} & -\frac{1}{4\pi}\int_{cell} d\vec{r}\,\{\Sigma^{*g}_{tr}-\Sigma^{g}_{tr}(\vec{r})\}\,\Psi_{0}^{*g}\Phi_{0}^{g}(\vec{r}) \\ = & -\frac{1}{4\pi}\int_{cell} d\vec{r}\,\{\Sigma^{*g}_{a}-\Sigma^{g}_{a}(\vec{r})\}\,\Psi_{0}^{*g}\Phi_{0}^{g}(\vec{r}) \\ & -\frac{1}{4\pi}\int_{cell} d\vec{r}\,\{\Sigma^{*g}_{s}-\Sigma^{g}_{s}(\vec{r})\}\,\Psi_{0}^{*g}\Phi_{0}^{g}(\vec{r}) \end{aligned} \qquad (A.4)$$

Then the second term becomes

$$
\begin{aligned}
&-\frac{1}{4\pi}\int_{cell} d\vec{r}\ \{\Sigma_a^{*g}-\Sigma_a^g(\vec{r})\}\ \Psi_0^{*g}\Phi_0^g(\vec{r}) \\
&+\frac{1}{4\pi}\int_{cell} d\vec{r}\sum_{g'}\Sigma_s^{*g\to g'}\Phi_0^g\{\Psi_0^{*g'}(\vec{r})-\Psi_0^{*g}(\vec{r})\} \\
&-\sum_{g'}\Sigma_s^{*g\to g'}\Phi_0^g\{\Psi_0^{*g'}(\vec{r})-\Psi_0^{*g}(\vec{r})\}
\end{aligned}
\qquad (A.5)
$$

The first term becomes

$$
\begin{aligned}
&-\int_{cell} d\vec{r}\int d\vec{\Omega}\ \{\Sigma_{tr}^{*g}-\Sigma_{tr}^g(\vec{r})\}\ \Phi^g(\vec{r},\vec{\Omega})\ \Psi^{*g}(\vec{r},\vec{\Omega}) \\
&+\frac{1}{4\pi}\int_{cell} d\vec{r}\ \{\Sigma_{tr}^{*g}-\Sigma_{tr}^g(\vec{r})\}\ \Phi_0^g(\vec{r})\ \Psi_0^{*g}(\vec{r}) \\
&=-\int_{cell} d\vec{r}\int d\vec{\Omega}\,\Sigma_{tr}^{*g}\{\Phi^g(\vec{r},\vec{\Omega})\ \Psi^{*g}(\vec{r},\vec{\Omega})-\frac{1}{4\pi}\Phi_0^g(\vec{r})\ \Psi_0^{*g}(\vec{r})\} \\
&\quad+\int_{cell} d\vec{r}\int d\vec{\Omega}\sum_{g'}\Sigma_{tr}^g(r)\ \{\Phi^g(\vec{r},\vec{\Omega})\ \Psi^{*g}(\vec{r},\vec{\Omega})-\frac{1}{4\pi}\Phi_0^g(\vec{r})\ \Psi_0^{*g}(\vec{r})\}
\end{aligned}
\qquad (A.6)
$$

Substituting Eqs.(A.5) and (A.6) into Eq.(A.3), and setting each term on the right side of Eq.(A.3) to zero, we obtain

$$
\Sigma_a^{*g}=\frac{\int_{cell} d\vec{r}\ \Sigma_a^g(\vec{r})\ \Phi_0^g(\vec{r})\ \Psi_0^{*g}(\vec{r})}{\int_{cell} d\vec{r}\ \Phi_0^g(\vec{r})\ \Psi_0^{*g}(\vec{r})} \qquad (A.7)
$$

$$
\Sigma_s^{*g\text{-}g'}=\frac{\int_{cell} d\vec{r}\ \Sigma_s^{g\text{-}g'}(\vec{r})\ \Phi_0^g(\vec{r})\ \{\Psi_0^{*g'}(\vec{r})-\Psi_0^{*g}(\vec{r})\}}{\int_{cell} d\vec{r}\ \Phi_0^g(\vec{r})\ \{\Psi_0^{*g'}(\vec{r})-\Psi_0^{*g}(\vec{r})\}} \qquad (A.8)
$$

$$
\nu\Sigma_f^{*g}=\frac{\int_{cell} d\vec{r}\ \nu\Sigma_f^g(\vec{r})\ \Phi_0^g(\vec{r})\sum_{g'}\chi^{g'}\Psi_0^{*g'}(\vec{r})}{\int_{cell} d\vec{r}\ \Phi_0^g(\vec{r})\sum_{g'}\chi^{g'}\Psi_0^{*g'}(\vec{r})} \qquad (A.9)
$$

$$
\Sigma_{tr}^{*g}=\frac{\int_{cell} d\vec{r}\int d\vec{\Omega}\,\Sigma_{tr}^g(\vec{r})\ \{\Phi(\vec{r},\vec{\Omega})-\frac{1}{4\pi}\Phi_0^g(\vec{r})\}\ \Psi^{*g}(\vec{r},\vec{\Omega})}{\int_{cell} d\vec{r}\int d\vec{\Omega}\ \{\Phi(\vec{r},\vec{\Omega})-\frac{1}{4\pi}\Phi_0^g(\vec{r})\}\ \Psi^{*g}(\vec{r},\vec{\Omega})} \qquad (A.10)
$$

Eq.(A.10) is somewhat difficult to understand the physical meaning. Therefore we transform Eq.(A.10) and compare the resultant transport cross section with the Benoist's DC and the extended Benoist DC.

Let us express the adjoint angular flux by the P_1 approximation.

$$\Psi^{*g}(\vec{r},\vec{\Omega}) = \frac{1}{4\pi}\left[\Psi_0^{*g}(\vec{r}) + 3\vec{\Omega}\cdot\vec{\Psi}_1^{*g}(\vec{r})\right] \tag{A.11}$$

This approximation is reasonable because after the cell homogenization the angular flux anisotropy becomes small. Substitution of Eq.(A.11) into Eq.(A.10) leads to

$$\Sigma_{tr}^{*g} = \frac{\int_{cell} d\vec{r}\ \Sigma_{tr}^{g}(\vec{r})\ \{\vec{\Psi}_1^{*g}(\vec{r})\cdot\vec{\Phi}_1^{g}(\vec{r})\}}{\int_{cell} d\vec{r}\ \{\vec{\Psi}_1^{*g}(\vec{r})\cdot\vec{\Phi}_1^{g}(\vec{r})\}} \tag{A.12}$$

where $\vec{\Phi}_1^{g}(\vec{r})$ is the P_1 component of the neutron angular flux. The above definition of the transport cross section guarantees the preservation of total neutron leakage. To treat the diffusion anisotropy we preserve the neutron leakage in each direction by using the direction dependent cross section defined by

$$\Sigma_{tr,k}^{*g} = \frac{\int_{cell} d\vec{r}\ \Sigma_{tr}^{g}(\vec{r})\ \Psi_{1,k}^{*g}(\vec{r})\ \Phi_{1,k}^{g}(\vec{r})}{\int_{cell} d\vec{r}\ \{\Psi_{1,k}^{*g}(\vec{r})\ \Phi_{1,k}^{g}(\vec{r})\}} \tag{A.13}$$

Here let us consider how the DC is utilized in fast reactor core calculations in predicting core parameters. The parameters are commonly calculated by performing diffusion calculations with Benoist's DC, and adding a transport correction to the results. The transport correction is obtained by the difference between the core parameters obtained from a diffusion calculation with an appropriate DC and a transport calculations with a transport cross section defined by $\Sigma_{tr}=1/3DC$. Thus when we use the transport cross section defined by Eq.(A.13) in the transport calculation, we should use the anisotropic DC defined by

$$D_k^{*g} = \frac{1}{3\Sigma_{tr,k}^{*g}} = \frac{\int_{cell} d\vec{r}\ \Phi_{1,k}^{g}(\vec{r})\ \Psi_{1,k}^{*g}(\vec{r})}{3\int_{cell} d\vec{r}\ \Sigma_{tr}^{g}(\vec{r})\ \Phi_{1,k}^{g}(\vec{r})\ \Psi_{1,k}^{*g}(\vec{r})} \tag{A.14}$$

In the following we obtain an explicit form of Eq.(A.13) for an infinite lattice and a multidrawer cell model, and compare the resultant form with the Benoist's DC and the extended Benoist DC.

First let us consider an infinite lattice where the same cell is repeated infinitely. In this case the adjoint angular flux is constant over a cell after the cell homogenization. The forward angular flux is approximated by the product of a global flux distribution $\exp(i\vec{B}\cdot\vec{r})$ and the microscopic flux distribution $\phi^{g}(\vec{r},\vec{\Omega})$ expressing the intra-cell flux distribution :

$$\Phi^{g}(\vec{r},\vec{\Omega}) = \exp(i\vec{B}\cdot\vec{r})\ \phi^{g}(\vec{r},\vec{\Omega}) \tag{A.15}$$

The microscopic distribution is divided into real and imaginary parts as follows :

$$\phi^{g}(\vec{r},\vec{\Omega}) = \phi^{R,g}(\vec{r},\vec{\Omega}) + i\vec{B}\cdot\vec{\phi}^{I,g}(\vec{r},\vec{\Omega}) \qquad (A.16)$$

where $\vec{\varphi}^{I,g}(\vec{r},\vec{\Omega})$ is a vector having the component $\varphi^{Ik,g}(\vec{r},\vec{\Omega})$ in the k-th direction. Substituting Eqs.(A.15) and (A.16) into the transport equation and equating the real and imaginary parts of the right and left hand-sides we obtain the relations

$$\vec{\Omega}\cdot grad\,\phi^{R,g}(\vec{r},\vec{\Omega}) + \Sigma^{g}_{tr}(\vec{r})\,\phi^{R,g}(\vec{r},\vec{\Omega}) - (\vec{B}\cdot\vec{\Omega})\,(\vec{B}\cdot\vec{\phi}^{I,g}(\vec{r},\vec{\Omega}))$$

$$= \sum_{g'}\int d\vec{\Omega}'\,\Sigma_{s}^{g'\to g}(\vec{r})\,\phi^{R,g'}(\vec{r},\vec{\Omega}) + \frac{\chi^{g}}{4\pi k_{eff}}\sum_{g'}\nu\Sigma_{f}^{g'}(\vec{r})\int d\vec{\Omega}'\,\phi^{R,g'}(\vec{r},\vec{\Omega}) \qquad (A.17)$$

and

$$\vec{\Omega}\cdot grad\,\phi^{Ik,g}(\vec{r},\vec{\Omega}) + \Sigma^{g}_{tr}(r)\,\phi^{Ik,g}(\vec{r},\vec{\Omega}) + \Omega_{k}\phi^{R,g}(\vec{r},\vec{\Omega})$$

$$= \sum_{g'}\Sigma_{s}^{g'\to g}(\vec{r})\int d\vec{\Omega}'\,\phi^{Ik,g'}(\vec{r},\vec{\Omega}') + \frac{\chi^{g}}{4\pi k_{eff}}\sum_{g'}\nu\Sigma_{f}^{g'}(\vec{r})\int d\vec{\Omega}'\,\phi^{Ikg'}(\vec{r},\vec{\Omega}) \qquad (A.18)$$

$$(k=x,\ y,\ z)$$

From Eq.(A.15) the P_1 component of the angular flux is given by

$$\varphi^{g}_{1k}(\vec{r}) = exp\,(i\vec{B}\cdot\vec{r})\,\{\phi^{R,g}_{1k}(\vec{r}) + i\sum_{k'}B_{k'}\phi^{1k'\cdot g}_{1k}(\vec{r})\}. \qquad (A.19)$$

When a cell is symmetric about its center, the P_1 component of the real part is antisymmetric. Therefore,

$$\int_{cell}d\vec{r}\,\phi^{R,g}_{1k}(\vec{r}) = 0 \quad for\ all\ k. \qquad (A.20)$$

Similarly for the P_1 component of the imaginary part,

$$\int_{cell}d\vec{r}\,\phi^{Ik,g}_{1k'}(\vec{r}) = 0 \quad for\ all\ k=k'. \qquad (A.21)$$

On the contrary $\varphi^{Ik,g}_{1k}(\vec{r})$ is symmetric about a cell center because $\varphi^{Ig}(\vec{r},\vec{\Omega})$ has a source term $-\Omega_{k}\varphi^{R,g}(\vec{r},\vec{\Omega})$ as shown in Eq.(A.18). Thus, only $\varphi^{Ik,g}_{1k}(\vec{r})$ remains if we take the cell average of $\varphi^{g}_{1k}(\vec{r})$ neglecting the change in the global distribution in a cell, therefore Eq.(A.14) is reduced to

$$D^{*g}_{k} = \frac{\int_{cell}d\vec{r}\,\phi^{Ik,g}_{1k}(\vec{r})}{3\int_{cell}d\vec{r}\,\Sigma^{g}_{tr}(\vec{r})\,\phi^{Ik,g}_{1k}(\vec{r})} \qquad (A.22)$$

Transforming the above equation through the integral transport theory using the procedure shown in Reference[6] we obtain

$$D^{*g}_{k} = \frac{\sum_{j\in cell}\sum_{i\in cell}\phi^{R,g}_{0,i}V_{i}P^{g}_{ij,x}/3\Sigma^{g}_{tr,j}}{\sum_{i\in cell}\phi^{R,g}_{0,i}V_{i}} \qquad (A.23)$$

This is the commonly used Benoist's formula for the anisotropic diffusion coefficient.

Thus, for infinite uniform lattices, the derived cross sections reduce to the commonly used flux-weighted ones, and the derived anisotropic diffusion coefficient reduces to Benoist's formula. This agreement if the present formula to the commonly used homogenization procedure indicates that the conventional procedure is correct at least around a core center where the

global flux distribution is well approximated by $\exp(i\vec{B}\cdot\vec{r})$. Next let us consider an 1-D multidrawer cell model containing several different types of cells.

For the calculation of the anisotropic DC defined by Eq.(A.14) it is necessary to calculate the P_1 components of the forward and adjoint angular fluxes. In the 1-D model the P_1 component in the direction perpendicular to plates is not zero, but zero in the parallel direction. Therefore a separate treatment is necessary for the parallel and perpendicular DCs.

Let us choose the x and z axes in the perpendicular and parallel directions, respectively. In heterogeneous lattices the flux distribution along the x-axis becomes complicated and can not be expressed by an asymptotic one, but that along the z-axis is assumed to have the form proportional to $\exp(iB_z\cdot z)$. The same is true for the other parallel direction (y-axis), but for simplicity, the parallel direction is represented by only the z-axis. Thus the forward and adjoint angular flux distributions can be written as follows :

$$\Phi^g(x,\ z,\ \vec{\Omega}) = \exp(iB_z\cdot z)\ \{\phi^{R,g}(x,\ \vec{\Omega}) + iB_z\phi^{1z,g}(x,\ \vec{\Omega})\} \qquad (A.24)$$

and

$$\Psi^g(x,\ z,\ \vec{\Omega}) = \exp(-iB_z\cdot z)\ \{\psi^{*R,g}(x,\ \vec{\Omega}) + iB_z\psi^{*1z,g}(x,\ \vec{\Omega})\}. \qquad (A.25)$$

The z-direction P_1 components of $\varphi^{R,g}(x,\vec{\Omega})$ and $\psi^{*R,g}(x,\vec{\Omega})$ are zero,because the angular distributions of $\varphi^{R,g}(x,\vec{\Omega})$ and $\psi^{*R,g}(x,\vec{\Omega})$ are symmetric about the x-axis. Therefore, the parallel diffusion coefficient is given by

$$D_{//}^{*g} = \frac{\sum_{i\in cell} \phi^{1,g}_{1z,i}\psi^{*1,g}_{1z,i}V_i}{3\sum_{i\in cell}\Sigma^g_{tr,i}\phi^{1,g}_{1z,i}\psi^{*1,g}_{1z,i}V_i} \qquad (A.26)$$

where $\varphi^{I,g}_{1z,i}$ and $\psi^{*I,g}_{1z,i}$ are the z-direction P_1 components of the imaginary parts of Eqs (A.24) and (A.25) in region i. The perpendicular diffusion coefficient is given by

$$D_{\perp}^{*g} = \frac{\sum_{i\in cell} \phi^{g}_{1x,i}\psi^{g}_{1x,i}V_i}{3\sum_{i\in cell}\Sigma^g_{tr,i}\phi^{g}_{1x,i}\psi^{g}_{1x,i}V_i} \qquad (A.27)$$

where $\Phi^g_{1x,i}$ and $\Psi^{*g}_{1x,i}$ are the x-direction P_1 components of the forward and adjoint angular distributions in region i.

In the following we compare the expressions for the parallel and perpendicular DC with the extended Benoist DC. We express $\Phi^{I,g}_{1z,i}$ and $\Phi^g_{1x,i}$ with the collision probabilities as derived in Reference[6]. The parallel DC is reduced to

$$D_{//}^{*g} = \frac{\sum_{j \in \text{supercell}} \sum_{i \in \text{cell}} P_{ji,z}^{g} \, \phi_{0,j}^{R,g} \, V_j \, \psi_{1z,i}^{g} \, / 3 \, \Sigma_{tr,i}^{g}}{\sum_{j \in \text{supercell}} \sum_{i \in \text{cell}} P_{ji,z}^{g} \, \phi_{0,j}^{R,g} \, V_j \, \psi_{1z,i}^{g}} \qquad \text{(A.28)}$$

If we neglect the spatial variation of $\psi_{1z,i}^{*I,g}$, we obtain

$$D_{//}^{*g} = \frac{\sum_{j \in \text{supercell}} \sum_{i \in \text{cell}} P_{ji,z}^{g} \, \phi_{0,j}^{R,g} \, V_j \, / 3 \, \Sigma_{tr,i}^{g}}{\sum_{j \in \text{supercell}} \sum_{i \in \text{cell}} P_{ji,z}^{g} \, \phi_{0,j}^{R,g} \, V_j} \qquad \text{(A.29)}$$

while the extended Benoist parallel DC is defined by

$$D_{//,\text{extend}}^{*g} = \frac{\sum_{j \in \text{supercell}} \sum_{i \in \text{cell}} P_{ji,z}^{g} \, \phi_{0,j}^{R,g} \, V_j \, / 3 \, \Sigma_{tr,i}^{g}}{\sum_{i \in \text{cell}} \phi_{0,i}^{R,g} \, V_i} \qquad \text{(A.30)}$$

The numerator of the above equation is the same as that of Eq.(A.27), but the denominator is different.

Table I Energy Structure for 7 Groups

Energy Group	Upper-energy	
1	10.0	(MeV)
2	3.6788	
3	1.3534	
4	86.517	(keV)
5	9.1188	
6	961.12	(eV)
7	101.30	

Table II Comparison of k_{eff} for the reference calculation and the four homogenization methods

	model(a)	model(b)	model(c)
Methods	k_{eff}	k_{eff}	k_{eff}
Reference	0.9896	1.0361	0.4608
Homogenization Methods (1)	0.9856 (-0.40)*	1.0339 (-0.21)	0.3907 (-3.96)
(2)	0.9882 (-0.14)	1.0354 (-0.07)	0.4037 (-0.76)
(3)	0.9896 (0.00)	1.0361 (0.00)	0.4068 (0.00)
(4)	0.9901 (0.05)	1.0367 (0.06)	0.4069 (0.02)

	model(d)	model(c')	model(d')
Methods	k_{eff}	k_{eff}	k_{eff}
Reference	0.6134	0.4100	0.6169
Homogenization Methods (1)	0.6037 (-1.58)	0.3938 (-3.95)	0.6067 (-1.65)
(2)	0.6117 (-0.28)	0.4066 (-0.83)	0.6147 (-0.36)
(3)	0.6134 (0.00)	0.4100 (0.00)	0.6169 (0.00)
(4)	0.6140 (0.10)	0.4107 (0.17)	0.6178 (0.15)

* percent deviation from the reference

Table III Comparison of DCs for model (b) Fuel+Fuel+CRP

i) Fuel (not adjacent to CRP)

Energy Group	method (1) $D_\perp$	method (1) $D_{//}$	method (2) $D_\perp$	method (2) $D_{//}$	method (3) D^{*2}	method (4) $D_\perp$	method (4) $D_{//}$
1	0.78*1	0.87	0.87	0.65	-0.80	-0.10*3	0.84
2	0.55	0.73	3.59	1.59	-0.43	-0.08	0.71
3	0.12	0.38	2.96	1.03	-0.04	-0.02	0.38
4	0.25	0.87	1.28	1.07	0.11	-0.01	0.87
5	3.21	7.95	3.47	8.03	0.28	0.02	7.99
6	0.14	1.40	1.75	1.86	0.38	0.02	2.04
7	-0.42	1.55	1.86	2.23	0.85	0.05	1.62

ii) Fuel (adjacent to CRP)

Energy Group	method (1) $D_\perp$	method (1) $D_{//}$	method (2) $D_\perp$	method (2) $D_{//}$	method (3) D^{*2}	method (4) $D_\perp$	method (4) $D_{//}$
1	0.78*1	0.87	11.51	8.79	-2.54	3.17	0.89
2	0.55	0.73	17.09	12.37	-1.26	2.50	0.88
3	0.12	0.38	23.47	14.36	-0.09	-0.88	0.73
4	0.25	0.87	18.24	10.29	0.12	1.10	1.21
5	3.21	7.95	11.06	11.41	0.25	-0.49	8.33
6	0.14	1.40	18.92	10.37	-0.09	0.13	2.06
7	-0.42	1.55	22.48	12.50	-0.93	0.59	1.84

iii) CRP

Energy Group	method (2) $D_\perp$	method (2) $D_{//}$	method (3) D^{*2}	method (4) $D_\perp$	method (4) $D_{//}$
1	-16.37*4	-11.07	9.32	8.56	0.59
2	-24.85	-15.16	4.98	7.61	0.50
3	-26.71	-14.26	0.75	5.00	0.43
4	-18.02	- 8.21	-0.23	- 9.49	0.95
5	- 6.15	- 1.92	-0.93	- 2.31	0.83
6	-15.07	- 5.00	-2.60	-10.09	2.55
7	-16.21	- 5.50	-5.67	- 9.68	2.47

*1 percent difference from $1/3\Sigma_{tr}$ where Σ_{tr} is the flux weighted transport cross section obtained from the infinite cell calculation

*2 $1/3\Sigma_{tr}$ where Σ_{tr} is the transport cross section by reaction rate preservation method obtained from the supercell calculation

*3 The term in the bracket [ ] in Eq.(5) was replaced by $\Phi_0^g(\vec{r})$.

*4 percent difference from $1/3\Sigma_{tr}$ where Σ_{tr} is the flux weighted transport cross section obtained from the supercell calculation

Table IV Comparison of DCs for model (d) Fuel+Fuel+CR

i) Fuel (not adjacent to CR)

Energy Group	method (1) $D_\perp$	$D_{//}$	method (2) $D_\perp$	$D_{//}$	method (3) D^{*2}	method (4) $D_\perp$	$D_{//}$
1	0.78*1	0.87	-5.07	-1.91	0.32	-0.21*3	0.79
2	0.55	0.73	-3.02	-0.59	0.29	-0.20	0.65
3	0.12	0.38	-0.75	0.42	0.06	-0.13	0.32
4	0.25	0.87	-0.05	1.19	-0.08	-0.14	0.81
5	3.21	7.95	0.06	5.05	-0.82	-0.40	7.76
6	0.14	1.40	-1.55	0.61	-2.04	-0.11	1.95
7	-0.42	1.55	-0.78	2.19	-4.45	-0.15	1.45

ii) Fuel (adjacent to CR)

Energy Group	method (1) $D_\perp$	$D_{//}$	method (2) $D_\perp$	$D_{//}$	method (3) D^{*2}	method (4) $D_\perp$	$D_{//}$
1	0.78*1	0.87	-7.72	-3.60	-1.97	1.52	1.10
2	0.55	0.73	-5.09	-1.82	-1.25	1.17	0.77
3	0.12	0.38	-0.51	0.80	-0.37	0.16	0.21
4	0.25	0.87	0.15	1.34	-0.14	0.09	0.23
5	3.21	7.95	0.37	6.23	-1.42	2.11	4.74
6	0.14	1.40	-5.17	-0.12	-2.39	-0.26	0.29
7	-0.42	1.55	-7.47	1.32	-4.79	-2.07	-2.28

iii) CR

Energy Group	method (2) $D_\perp$	$D_{//}$	method (3) D^{*2}	method (4) $D_\perp$	$D_{//}$
1	20.87*4	10.54	3.32	0.00	1.15
2	11.48	6.59	1.46	25.81	2.08
3	1.96	4.84	0.14	8.26	5.17
4	1.70	5.13	0.04	4.73	5.45
5	5.17	2.86	1.30	- 0.98	0.54
6	25.95	18.88	2.59	8.12	9.09
7	58.82	42.51	11.45	11.01	12.72

*1 percent difference from $1/3\Sigma_{tr}$ where Σ_{tr} is the flux weighted transport cross section obtained from the infinite cell calculation

*2 $1/3\Sigma_{tr}$ where Σ_{tr} is the transport cross section by reaction rate preservation method obtained from the supercell calculation

*3 The term in the bracket [ ] in Eq.(5) was replaced by $\Phi_0^g(\vec{r})$.

*4 percent difference from $1/3\Sigma_{tr}$ where Σ_{tr} is the flux weighted transport cross section obtained from the supercell calculation

Table V Comparison of $D_{\perp}$ for the reactivity preservation method based on Eqs.(5) and (8) for the fuel drawer of model (a)

Energy Group	Eq.(5)	Eq.(8)
1	7.03*	1.22
2	6.62	0.84
3	0.96	-0.02
4	1.41	1.35
5	-2.10	5.43
6	1.38	0.53
7	3.69	-1.59

* percent difference from $1/3\Sigma_{tr}$ where Σ_{tr} is the infinite-cell flux weighted transport cross section

Table VI Cell-averaged cross section difference for the four methods for model (b) Fuel+Fuel+CRP

[I] absorption

Energy Group	i) Fuel (not adjacent to CRP) method (2)	method (3)	method (4)	ii) Fuel (adjacent to CRP) method (2)	method (3)	method (4)	iii) CRP method (3)	method (4)
1	0.56*1	1.27	0.57	1.74*1	3.95	1.79	-9.32*2	0.06
2	0.31	1.15	0.81	1.98	3.06	2.04	-4.98	0.04
3	0.29	0.31	0.32	0.45	0.52	0.50	-0.75	0.01
4	0.01	0.10	0.03	-0.00	-0.12	0.02	0.23	0.01
5	-0.06	-0.31	-0.03	-0.18	-0.34	-0.14	0.93	0.02
6	-0.20	-0.55	-0.15	-0.41	-0.28	-0.30	2.60	0.04
7	-0.32	-1.11	-0.25	-0.67	0.36	-0.45	5.67	0.04

[II] production

Energy Group	i) Fuel (not adjacent to CRP) method (2)	method (3)	method (4)	ii) Fuel (adjacent to CRP) method (2)	method (3)	method (4)
1	1.02*1	1.74	1.04	3.20*1	5.45	3.25
2	0.90	1.26	0.93	2.27	3.36	2.34
3	0.43	0.45	0.48	0.66	0.74	0.84
4	0.02	-0.09	0.08	-0.02	-0.13	0.17
5	-0.16	-0.41	-0.10	-0.45	-0.61	-0.24
6	-0.42	-0.77	-0.35	-0.84	-0.71	-0.59
7	-0.63	-1.42	-0.56	-1.31	0.29	-1.01

*1 percent difference from the infinite cell calculation
*2 percent difference from the supercell flux-weighting procedure

Table VII Cell-averaged cross section difference for the four methods for model (d) Fuel+Fuel+CR

[I] absorption

Energy Group	i) Fuel (not adjacent to CR) method (2)	method (3)	method (4)	ii) Fuel (adjacent to CR) method (2)	method (3)	method (4)	iii) CR method (3)	method (4)
1	1.04*1	0.55	1.11	1.07*1	2.91	1.04	-3.21	-0.65
2	1.78	1.33	1.93	1.48	2.62	1.53	-1.44	-0.37
3	1.61	1.47	1.95	1.46	1.75	1.53	-1.41	-0.59
4	0.30	0.32	0.66	0.34	0.42	0.37	-0.04	-1.75
5	0.38	1.04	0.83	0.74	1.83	0.28	-1.28	-7.83
6	0.46	2.49	0.99	0.95	3.31	-0.44	-2.52	-18.00
7	0.51	5.10	0.99	1.04	5.95	-0.74	-10.27	-33.14

[II] production

Energy Group	i) Fuel (not adjacent to CR) method (2)	method (3)	method (4)	ii) Fuel (adjacent to CR) method (2)	method (3)	method (4)
1	1.90*1	1.41	2.08	1.93*1	3.82	1.97
2	2.03	1.58	2.24	1.69	2.84	1.73
3	2.38	2.23	2.84	2.17	2.47	2.28
4	0.74	0.76	1.20	0.85	0.93	0.91
5	0.92	1.58	1.36	1.80	2.90	1.37
6	0.95	3.00	1.36	1.96	4.34	1.00
7	1.01	5.62	1.42	2.01	6.97	0.64

*1 percent difference from the infinite cell calculation
*2 percent difference from the supercell flux-weighting procedure

Table VIII Control rod worth and k_{eff} for 1-D slab core with CR cells with separeate B_4C plates (2-drawer model)

CR pattern	Reference	method(1)	method(2)	method(2')*2	method(3)	method(4)
withdrawn	0.9921	0.9907	0.9932	0.9911	0.9928	0.9932
[I]	0.8881 (10.48*1)	0.8860 (10.57)	0.8891 (10.48)	0.8885 (10.35)	0.8893 (10.43)	0.8889 (10.50)
[II]	0.8708 (12.23)	0.8680 (12.39)	0.8719 (12.21)	0.8717 (12.05)	0.8725 (12.12)	0.8716 (12.24)
[III]	0.9359 (5.66)	0.9339 (5.73)	0.9369 (5.67)	0.9328 (5.88)	0.9369 (5.63)	0.9363 (5.73)
all inserted	0.6811 (31.35)	0.6760 (31.77)	0.6822 (31.31)	0.6827 (31.12)	0.6839 (31.11)	0.6829 (31.24)

* 1 control rod worth (%dk/k)
* 2 flux-weighting method ; Σ_{tr} is defined by $1/3D_{ex}$ where D_{ex} is the extended Benoist DC.

Table IX Control rod worth and k_{eff} for 1-D slab core with CR cells with lumped B_4C plates (2-drawer model)

CR pattern	Reference	method(1)	method(2)	method(2')*2	method(3)	method(4)
withdrawn	0.9921	0.9907	0.9932	0.9911	0.9928	0.9932
[I]	0.8889 (10.40*1)	0.8865 (10.52)	0.8890 (10.49)	0.8925 (9.95)	0.8899 (10.36)	0.8896 (10.43)
[II]	0.8725 (12.06)	0.8694 (12.24)	0.8728 (12.12)	0.8727 (10.94)	0.8740 (11.97)	0.8741 (11.99)
[III]	0.9367 (5.58)	0.9345 (5.67)	0.9366 (5.70)	0.9365 (5.51)	0.9375 (5.57)	0.9370 (5.66)
all inserted	0.6847 (30.98)	0.6789 (31.47)	0.6850 (31.03)	0.7033 (29.04)	0.6870 (30.80)	0.6875 (30.78)

* 1 control rod worth (%dk/k)
* 2 flux-weighting method ; Σ_{tr} is defined by $1/3D_{ex}$ where D_{ex} is the extended Benoist DC.

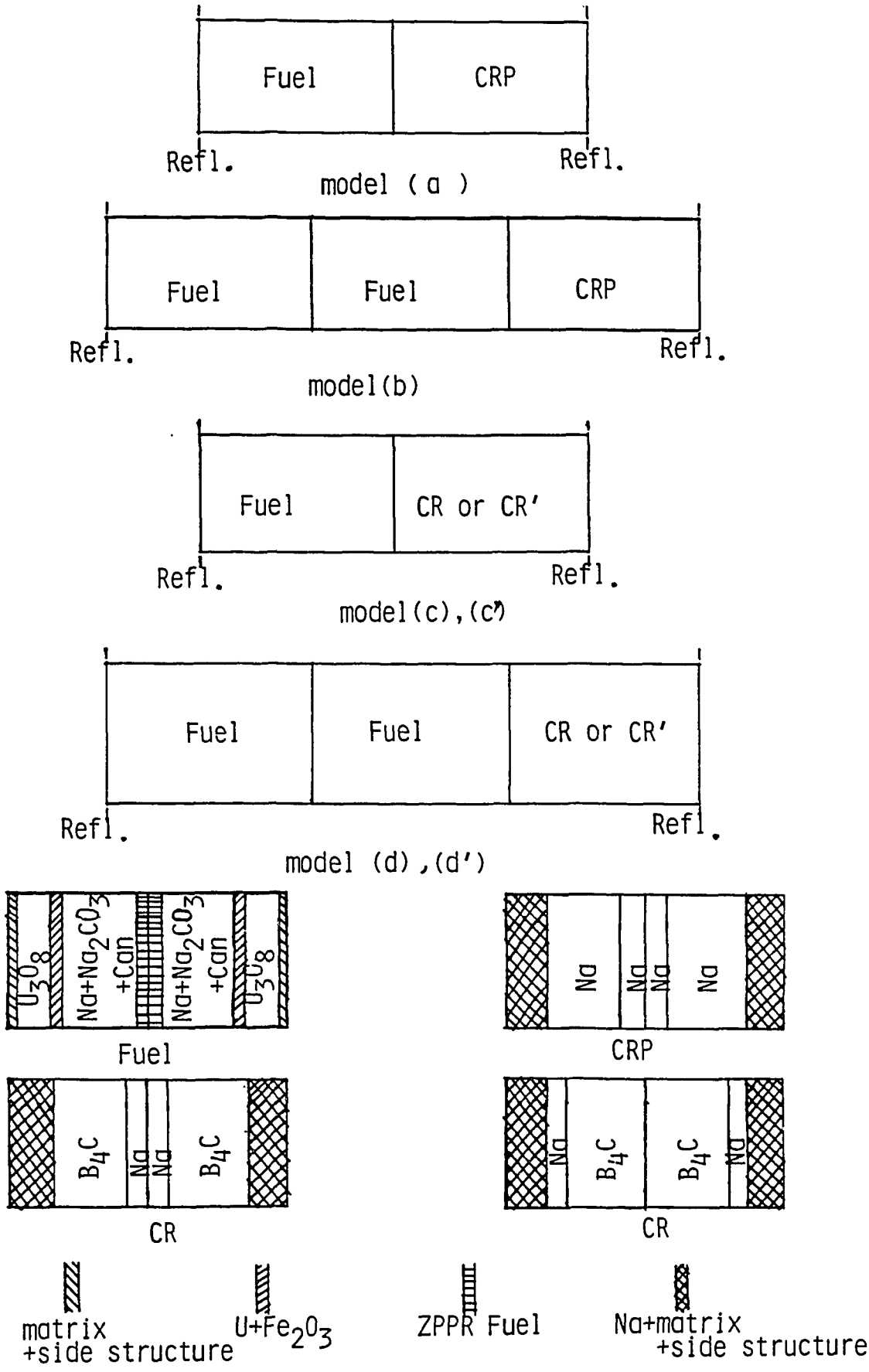

Fig. 1 Supercell models used for homogenization calculations

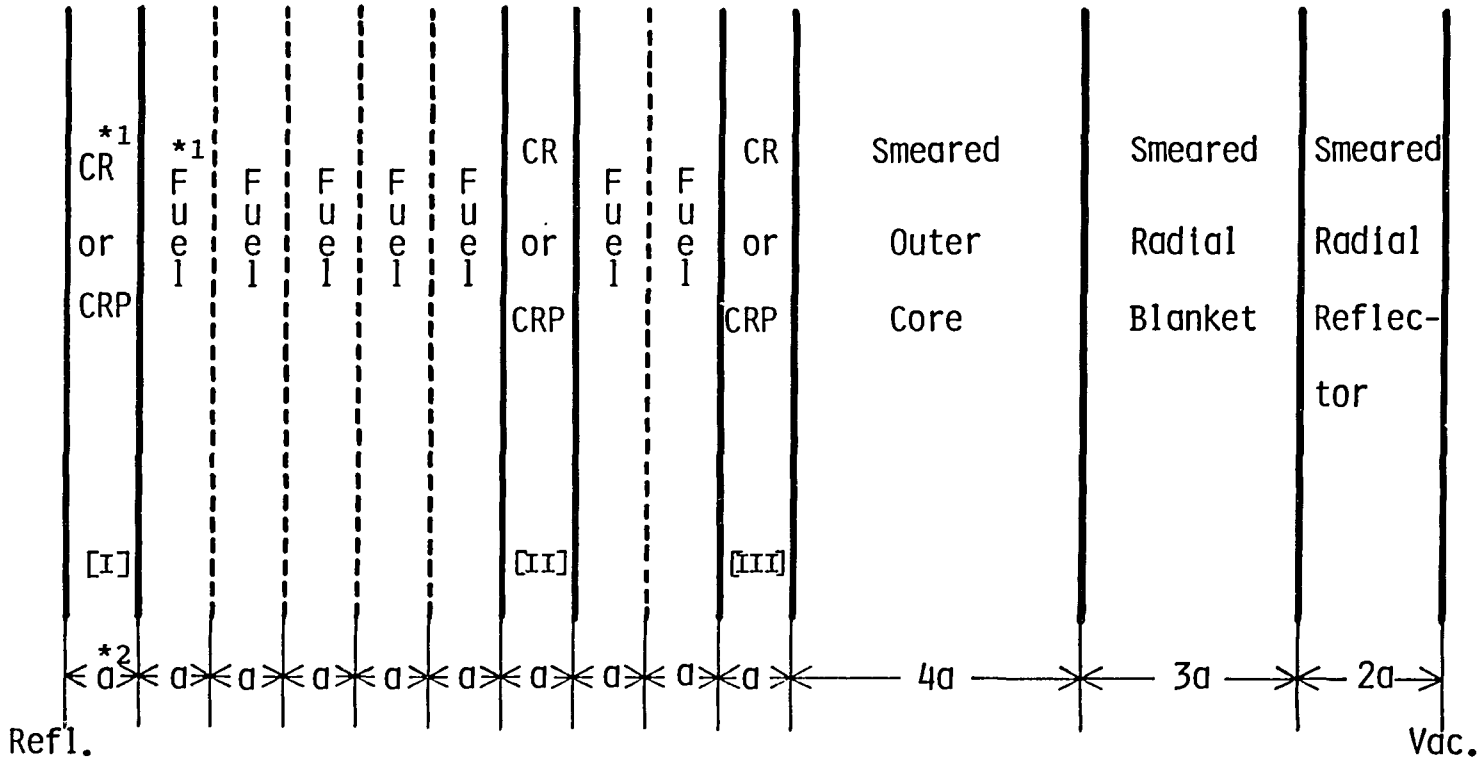

*1 The heterogeneous cell models as shown in Fig. 1 are used in the case of heterogeneous calculations

*2 a = 5.5245 (cm)

Fig. 2 1-D slab model for control rod worth calculations